Russian Geology and Geophysics © 2019, V.S. Sobolev IGM, Siberian Branch of the RAS
Vol. 60, No. 12, pp. 1407–1424, 2019 *DOI:10.15372/RGG2019136* *Geologiya i Geofizika*

Bastnaesite and Fluorite Rocks of the Ulan-Ude Occurrence (Mineral Composition, Geochemical Characteristics, and Genesis Issues)[1]

G.S. Ripp[a], I.R. Prokopyev[b,c], I.A. Izbrodin[a], E.I. Lastochkin[a], M.O. Rampilov[a, ✉], A.G. Doroshkevich[a,b], A.A. Redina[b], V.F. Posokhov[a], A.A. Savchenko[a], E.A. Khromova[a]

[a]*Geological Institute, Siberian, Branch of the Russian Academy of Sciences, ul. Sakhyanovoi 6a, Ulan-Ude, 670031, Russia*

[b]*Sobolev Institute of Geology and Mineralogy, Siberian Branch of the Russian Academy of Science, pr. Akademika Koptyuga 3, Novosibirsk, 630090, Russia*

[c]*Novosibirsk State University, Novosibirsk, ul. Pirogova 2, 630090, Russia*

Received 6 March 2018; received in revised form 21 May 2019; accepted 22 May 2019

Abstract—Within the city of Ulan-Ude, several sites of bastnaesite–fluorite rocks and calcite-containing rocks were found. They are confined to the exposures of Paleozoic schists and quartzites. The rocks have an age of 134.2 ± 2.6 Ma. They are brecciated lenticular and vein-like bodies cemented mainly with bastnaesite–fluorite aggregate. The content of fluorite in the rocks is several tens of percent, and the content of bastnaesite-(Ce) is 20–30%, often reaching 50%. Among the secondary minerals, there are monazite-(Ce), albite, and K-feldspar, and the accessory minerals are zircon, Nb-containing rutile, and manganilmenite. Light lanthanides are predominant among REE in the rocks. Bastnaesite and fluorite contain brine–melt fluid inclusions with homogenization temperatures of 490–520 ºC. The salts of these inclusions are composed of predominant Na and Ca sulphates and subordinate Ca and REE carbonates, and the gas phase contains CO_2. Gas inclusions and part of water–salt inclusions homogenized at 150–200, 290–350, and 430–450 ºC. The salts of late fluids are composed of Ca and REE carbonates, K and/or Na chlorides, Ca, Mg, and Fe hydrosulphates, and Ca and Na hydrocarbonates, and the gas phase contains $CO_2 \pm H_2$. The isotopic compositions of carbon (–5.9 to –8.3‰ $\delta^{13}C_{V\text{-}PDB}$) and oxygen (4.3 to 8.3‰ $\delta^{18}O_{V\text{-}SMOW}$) in bastnaesite and calcite fall in the PIC square specific to unaltered intrusive carbonatites. The primary strontium isotope ratios in fluorite and bastnaesite are equal to 0.70559–0.70568. The proximal location, close ages, and mineral and geochemical features indicate a genetic relationship of the studied rocks with the late Mesozoic carbonatites of southwestern Transbaikalia. The finding of this rock occurrence indicates a existence of one more carbonatite-bearing area and expands the distribution area of such rocks, which makes southwestern Transbaikalia promising for REE mineralization.

Keyword: rare-earth elements, bastnaesite, fluorite, fluid inclusions

INTRODUCTION

The bastnaesite-fluorite and calcite-rich rocks found within the city of Ulan-Ude contain high concentrations of rare-earth elements. They are represented by vein-shaped bodies and mineralized breccias with wide variations of xenoliths with different composition. Initially, the detected occurrence was classified as a hydrothermal formation (Ripp et al., 2018). After detection of rocks with bastnaesite content reaching 50% (Smolin district), and more detailed, including a thermobarogeochemical study, their high-temperature nature was determined. The proximity of the age, as well as the mineralogical and geochemical, including isotope characteristics of the identified symptoms with late Mesozoic carbonatite-bearing complexes of the Western Transbaikalia, permit to make the conclusion about their genetic connection.

There are several reasons for the publication of the proposed reports. One of them is associated with the appearance of another district including not so common specific rocks which are of interest to a wide range of specialists. The second reason is related to the uniqueness of their mineral and chemical composition. And, thirdly, the revealed occurrence with very high concentrations of rare-earth elements should cause interest as a forward-looking area for industrial rare-earth mineralization.

ANALYTICAL METHODS

The Ar/Ar age was determined by phlogopite, which is a typomorphic mineral of bastnaesite-containing rocks. The analysis was performed at Sobolev Institute of Geology and Mineralogy SB RAS (Novosibirsk) by the method of Travin

[1]This paper was translated by the authors

✉ Corresponding author.
E-mail adress: mrampilov@.mail.ru (M.O. Rampilov)

et al. (2009). The age plateau method was used in the calculation of the $^{39}Ar/^{40}Ar$ age (Fleck et al., 1977). According to the age plateau method, the weighted average age shall be calculated for several successive (not less than three) temperature levels.

Isotopic compositions of oxygen and carbon in calcite-bastnaesite and oxygen in silicates defined in the shared research center "Analytical Center for Mineralogical and Geochemical and Isotopic Studies" of the Geological Institute SB RAS (Ulan-Ude). The carbonates were decomposed using phosphoric acid with the GazBench option at a temperature of 60–70 °C for 2–4 hours. The measurements were carried out using the Finigan MAT 253 mass spectrometer in constant helium flow mode. Calibration for carbonates was performed according to NBS-18, NBS-19 standards (Friedman et al., 1982). The values $\delta^{13}C$ (V-PDB) and $\delta^{18}o$ (V-SMOW) were defined with an accuracy of ±0.05 and ±0.1‰ (1σ), respectively.

The oxygen from albite and phlogopite was isolated by a laser fluoridation method. The calibration of analyses was carried out according to international standards NBS-28 (quartz), NBS-30 (biotite) (Coplen, 1988). The method of analysis of silicate minerals is described in (Sharp, 1990). The error value of the analyses was ±0.1–0.3‰ at 95% confidence level.

Strontium isotopic relationships were defined in such "rubidium-free" minerals as fluorite and bastnaesite in the Analytical Center of mineralogical and geochemical and isotopic studies of the Geological Institute SB RAS (V.F. Posokhov) and the "Geodynamics and geochronology" Center of Collective Use of the Institute of the Earth's Crust SB RAS. Rb and Sr were isolated by standard method using ion-exchange resins. The isotopic compositions of Rb and Sr were measured on the Finnigan MAT 261 and TRITON multicollector mass spectrometers in a static mode. The accuracy of determining the concentrations of Rb and Sr made up ±0.5%, the isotopic ratios $^{87}Rb/^{86}Sr$ was ±0.5%, $^{87}Sr/^{86}Sr$ was ±0.05% (2σ).

Microstructural features, relationships and homogeneity of minerals were studied using a LEO-1430 electron microscope with the Inca Energy-300 energy dispersive spectrometer of E.A. Khromova.

The composition of rocks was determined by the methods of classical silicate analysis, X-ray fluorescence analysis (the Geological Institute SB RAS, Ulan-Ude). The high-resolution mass spectrometer with magnetic sector ELEMENT (Finnigan MAT) was used to determine the rare elements. To decompose the samples and convert them into a solution, the method of fusion with lithium metaborate developed at the analytical center of Sobolev Institute of Geology and Mineralogy SB RAS was used as the scientific basis. Detection limits of high-charge and rare-earth elements for most rare-earth elements make up between 0.01 and 0.06 ppm, for Eu, Ho, Lu—0.003 ppm, for high field strength elements—between 0.09 and 0.22 ppm.

Fluid inclusions were studied using optical microscopy (Olympus BX51 microscope), cryothermometry and Raman scattering spectroscopy methods. The cryothermometric studies were carried out in a THMSG-600 microthermometer made by Linkam. The composition of gas and salt phases of fluid inclusions was studied using the Raman scattering spectroscopy method: a Ramanor U-1000 spectrometer and a Horiba DU420E-OE-323 detector made by Jobin Yvon, a Millennia Pro laser device made by Spectra-Physics. The diagnostics of crystalline phases in the inclusions according to the Raman scattering spectroscopy data was carried out according to the database http://rruff.info. The chemical composition of the salt phases revealed in a dry system of fluid inclusions is determined by the method of scanning electron microscopy (SEM) with the JSM-6510 device, equipped with an energy-dispersion spectrometer (EDS) made by OXFORD. The number of thermometric experiments makes up about 60 analyses of fluid inclusions in fluorite and bastnaesite of different generations. The studies were carried out on the basis of the Center for collective use of scientific equipment for multi-element and isotopic studies at Sobolev Institute of Geology and Mineralogy SB RAS (Novosibirsk).

GEOLOGICAL STRUCTURE OF THE AREA OF THE ULAN-UDE OCCURRENCE

The occurrence is located in the northern part of the Mesozoic rift-related Ivolga–Uda depression (Fig. 1). According to the geological surveys (Platov et al., 2000), Late Cretaceous deposits (Sotnikovo Formation), represented by sandstones, siltstones, shales, conglomerates, lying on the eroded surface of the crystalline basement, are common here. The latter contains gneisses, migmatites, granite-gneisses, crystalline schists and limestones. The outcrops of these rocks are charted along the northern border of the cavity and in the outcrops on the right side of the Selenga River. The age of biotite amphibole gneisses occurring 15 km southerly of Ulan-Ude near the Oshurkovskoe apatite-bearing deposit is 282.8 ± 2.9 Ma (zircon, SHRIMP II) (Ripp et al., 2013, 2014). The metamorphic rocks are broken by granites and gneiss-granites, having according to a Rb–Sr geochronological study (Platov, 2000) ages between 277 and 314 Ma. The rocks, surrounding the cavity, are metamorphosed at the amphibolite facies level, and intensively tectonized, in some areas, they turned into breccias and are intersected by dislocations with breaks in continuity.

Biotite crystalline schists, quartzites, gneisses and breccias of these rocks are common on this occurrence area. Shales and gneisses consist mainly of plagioclase, potassium feldspar, biotite, quartz. Accessory minerals include titanite, rutile, zircon, apatite. The biotite from these rocks is characterized by a high ferruginosity (f_m > 60%) and a high alumina, it does not contain fluorine.

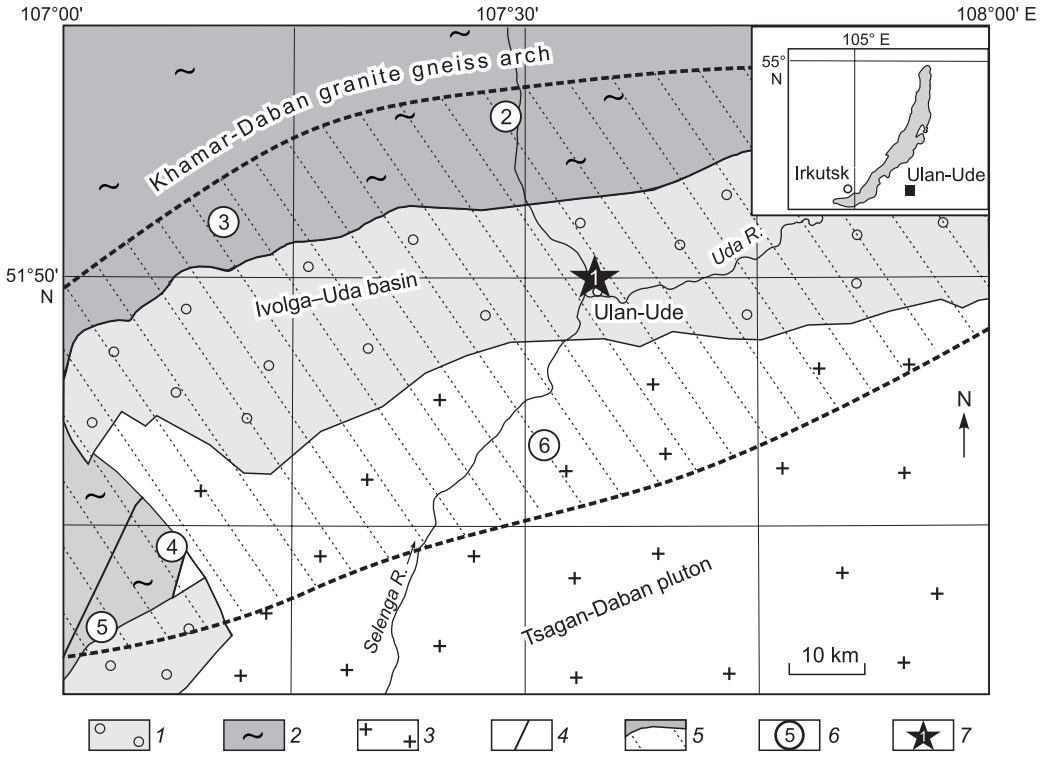

Fig. 1. The location of the Ulan-Ude occurrence and of the carbonatites in the South-Western Transbaikalia. The scheme of the tectonic structure by (Platov et al., 2000).

The bastnaesite-fluorite and calcite-containing rocks occur along the coastline of the Selenga River, in the rock outcrops, a ditch passed for the construction of underground utilities, and in the pits for the construction of houses within an erosion window strip 40–50 m wide and about 400 m long. To date, three sites have been established (Ulan-Ude, Portovyi and Smolin). All of them coincide with outcrops of Paleozoic metamorphic rocks overlapped by deposits of the Late Cretaceous. These rocks are part of a breccia with different types of clasts, which as a result of repeated crushing, was partially crushed to the size of 1–2 mm. During later tectonization, the mineralized areas were also fractionized and diluted with the materials of the host rocks. The occurrence is located within the Western Transbaikalian carbonatite province (Fig. 1) (Ripp et al., 2000). In 26–40 km to the west, to the southwest of it, calcite-rich carbonatites are located, which bear strontium (Khalyuta occurrence) and rare-earth (Arshan, Yuzhnoe occurrences) mineralization. The carbonatites were formed in the range between 135 and 122 Ma (Ripp et al., 2000) and they are controlled by a late Mesozoic rift-related structure.

For the determination of age, Ar–Ar isotopic studies of phlogopite were conducted, which was selected from bastnaesite and fluorite rocks (rock sample P-1) from the Portovyi site. The chemical composition of the mineral corresponds to tetraferriphlogopite. The results of $^{40}Ar/^{39}Ar$ dating are shown in Fig. 2. The stage heating graph of phlogopite shows a plateau with the age of 134.2 ± 2.6 Ma and the maximum fraction of cumulative ^{39}Ar. This value is accepted by us as the age of phlogopite and, accordingly, of bastnaesite-fluorite rocks formation.

Within the studied area, three structural-material epigenetic types of rocks are widespread: (1) lens-shaped and vein-like bastnaesite-fluorite bodies, (2) breccias cemented by the same mineral paragenesis (Figs. 3, 4) and (3) areas with calcite and albite-calcite associations containing bastnaesite and monazite (Fig. 5).

Areas of mineralized breccias occupy up to several square meters, surrounded by a metamorphic zone of phlo-

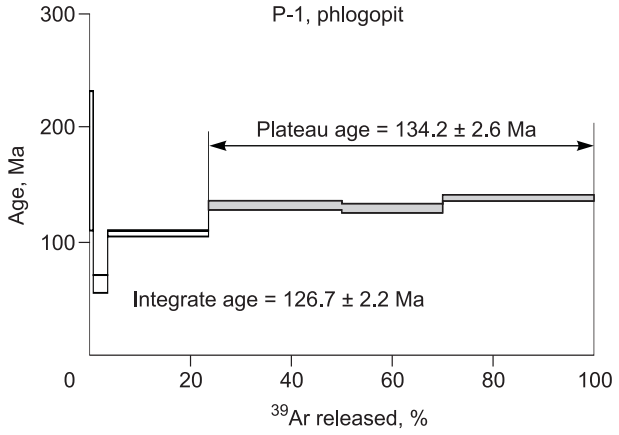

Fig. 2. $^{40}Ar/^{39}Ar$. The phlogopite spectrum of bastnaesite and fluorite rocks on the Portovoye site.

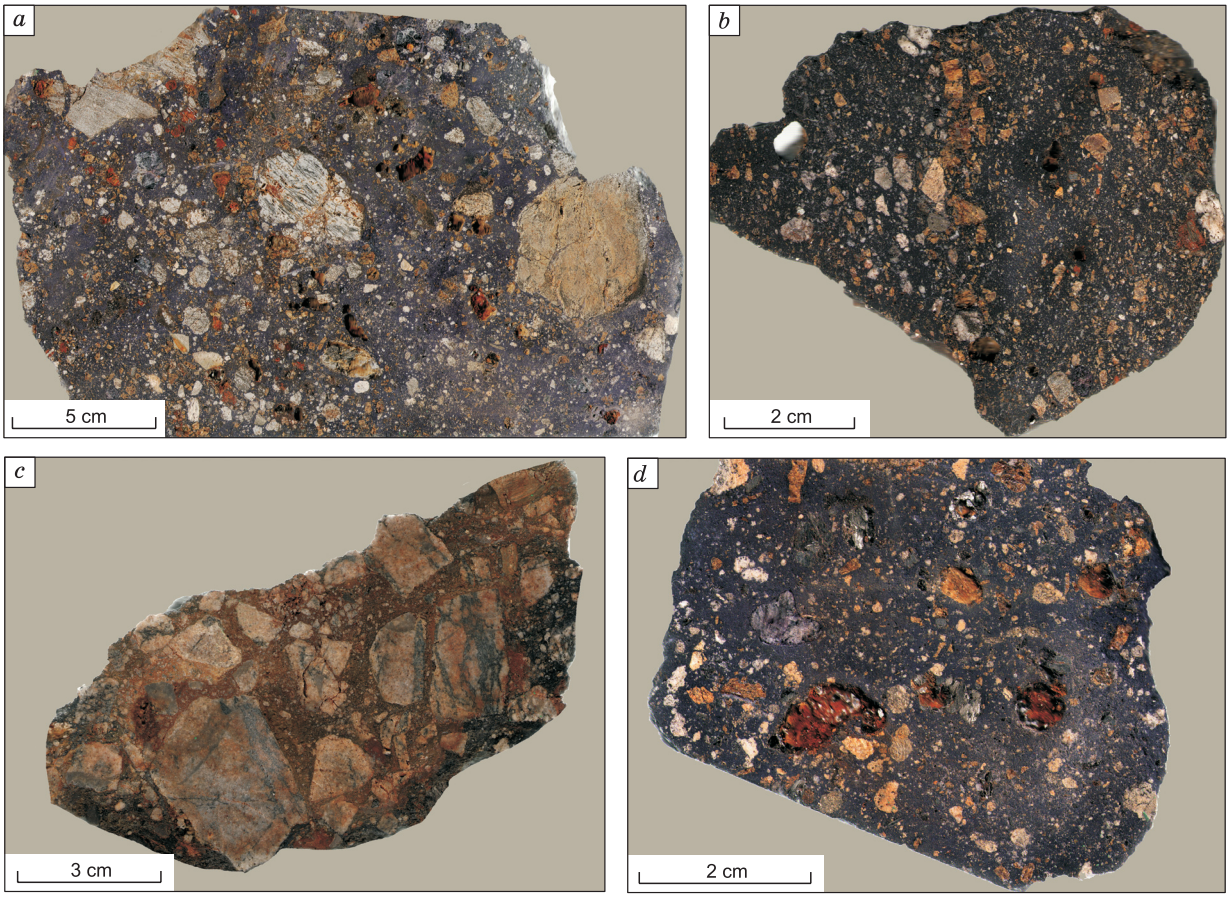

Fig. 3. The structural and textural features of breccia and massive fluorite-bastnaesite rocks on photographs of polished samples. The clastic material is represented by xenoliths of host schists and cemented by fine-grained bastnaesite-fluorite aggregate.

gopitization and thin bastnaesite-fluorite streaks. They contain numerous xenoliths of host rocks, the sizes of which may vary from 1–2 mm up to 10–15 cm. The breccias demonstrate banding around the xenoliths, accentuated orientation of the flakes of phlogopite and tabular grains of bastnaesite. Small fragments of disintegrated xenoliths have also been found on different spots. The newly formed minerals of the bastnaesite-fluorite association usually contain large amounts of xenogenic minerals (Fig. 4*a*). The xenoliths have sharp boundaries, and even small fragments do not show any significant hydrothermal alterations. The chemical composition is given in Table 1 (ans. 1, 2).

The width of the vein-like bodies usually does not exceed 0.5 m, their length—10 m. Their chemical composition is presented in Table 1 (ans. 3–6). On the contacts, they are edged with areas of anchimonomineral finely-scaled phlogopite with thickness of up to 1–2 cm. The phlogopitization zone can be traced at a distance of several meters from the orebodies, in the form of thin (up to filiform) streaks and monomineralic clusters.

Within the area of bastnaesite-fluorite rocks, calcite and albite-calcite rock associations were found. We did not observe any direct relationships with the host rocks due to poor exposure. The scale of occurrence of these fine-grained rocks containing scattered impregnation of bastnaesite, phlogopite and monazite is not determined. Visually, each of these sites covers an area of no more than the first square meters. The calcite together with the bastnaesite and the monazite fills the space between the grains of albite (Fig. 5); secondary minerals include apatite, rutile, muscovite, fluorite. The calcites always contain up to 1.5 wt.% of FeO and up to 3.6 wt.% of MnO. They rarely contain magnesium (less than 1 wt.% MgO). In the later calcite streaks, no impurity elements were found.

MINERAL COMPOSITION OF THE ROCKS

The bastnaesite-fluorite rocks are composed mainly of bastnaesite-(Ce) and fluorite (up to 30–55% each). Among the typomorphic mineral (5–10%), tetraferriphlogopite is present, and among secondary and accessory minerals: potassium feldspar, albite, zircon, manganilmenite, niobium-bearing rutile. Sulphate (3–4 wt.% SO_3) and phosphate (up to 1–1.5 wt.% P_2O_5) minerals are also typical, such as glauberite, plumbojarosite, monazite-(Ce), corkite. Disintegrated

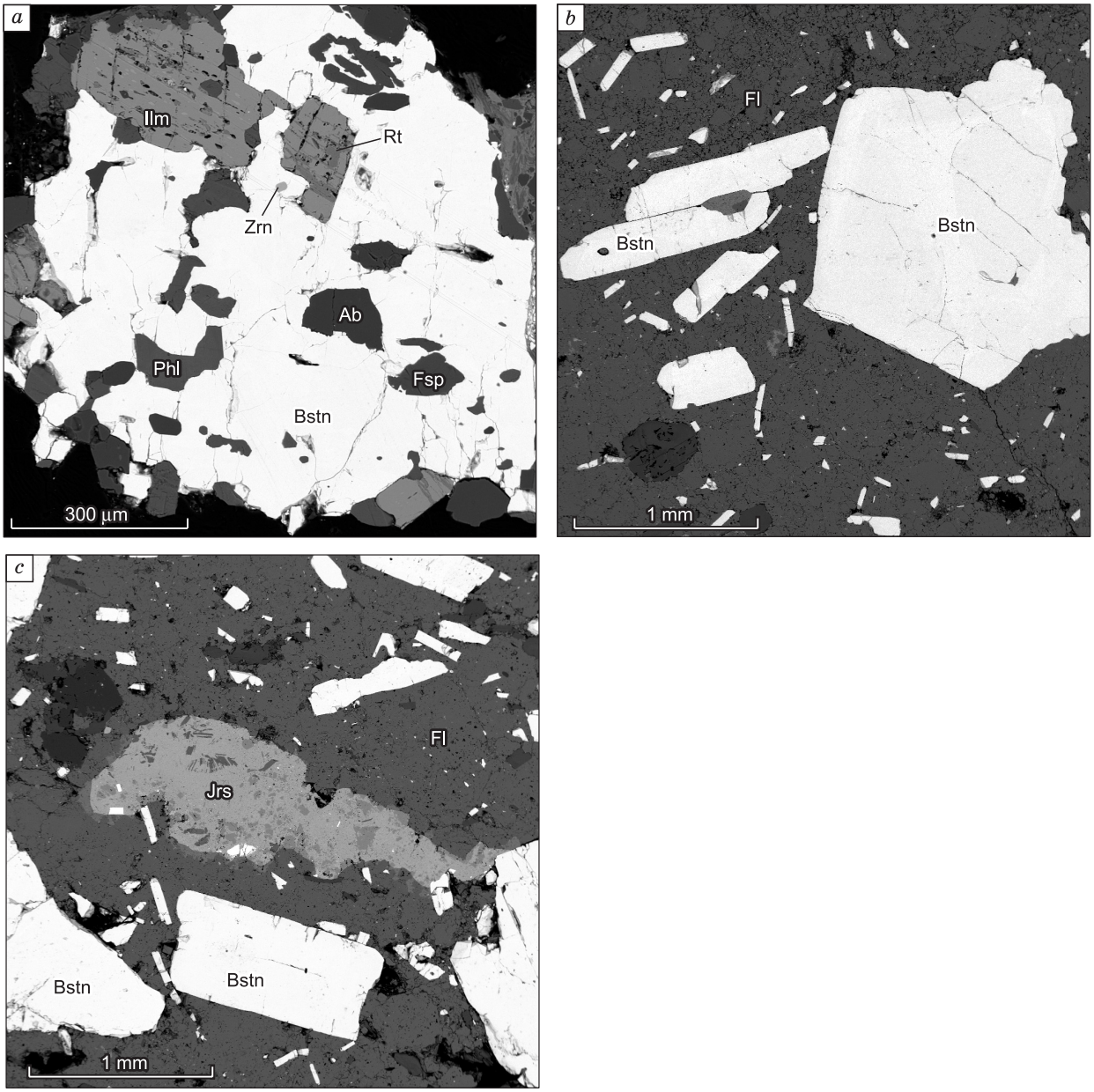

Fig. 4. The character of bastnaesite nodules in fluorite-bastnaesite rocks. *a*, Grains of bastnaesite with inclusions of xenoliths of feldspar and titanium-containing minerals; *b*, *c*, two generations of bastnaesite—phenocrysts and small tabular crystals in a fluorite matrix, the gray nest—fine-grained plumboyarozite. Bstn, bastnaesite; Fl, fluorite; Phl, phlogopite; Ab, albite; Zrn, zircon; Ilm, ilmenite; Fsp, potassium feldspar; Rt, rutile.

host rocks determined the presence of xenogenic quartz, albite, potassium feldspar and biotite.

Bastnaesite-(Ce) is represented in the rocks by two generations (Table 2). The early generation builds up phenocrysts of the size up to 1–1.5 cm. The grains of this generation are cut by streaks of fine-grained fluorite and a late plumbojarosite generation. In the inclusions of bastnaesite-(Ce) we found tetraferriphlogopite, plumbojarosite and glauberite. In the breccia rocks, bastnaesite-(Ce) often contains numerous inclusions of captured minerals (Fig. 4*a*). Among the latter, potassium feldspar, albite, titanium minerals, zircon are most often detected. In the mineral of early generation as a whole, the concentration of lanthanum is noticeably higher, and the concentration of neodymium is lower (Table 2, ans. 1–4).

The second generation is represented by small (2–4 mm) tabular grains scattered in a fine-grained fluorite matrix (Fig. 2*c*, *d*). Compared to the early bastnaesite the later one contains less cerium and more lanthanum (Table 2, ans. 5–12).

The bastnaesite-(Ce) from the calcite and albite-calcite association is close in morphological and chemical properties to the mineral from bastnaesite-fluorite rocks. The first one shows only a few large concentrations of neodymium.

Table 1. The chemical composition of bastnaesite and fluorite rocks

Element	1	2	3	4	5	6
	B-1/15a	B-1/15b	B-15-1	CM-1/18a	CM-2a/18	CM-3/18
SiO_2	66.10	46.70	n.d.	6.00	7.70	n.d.
TiO_2	0.27	0.37	n.d.	0.12	0.15	n.d.
Al_2O_3	13.04	9.57	n.d.	1.20	1.70	n.d.
Fe_2O_3	4.85	3.56	n.d.	1.49	0.82	n.d.
MnO	0.04	0.06	n.d.	0.01	0.01	n.d.
MgO	0.90	1.17	n.d.	1.01	0.89	n.d.
CaO	2.36	12.53	n.d.	48.30	51.80	n.d.
Na_2O	4.87	3.94	n.d.	0.35	0.52	n.d.
K_2O	3.79	2.39	n.d.	0.95	1.02	n.d.
P_2O_5	0.16	0.05	n.d.	0.14	0.17	n.d.
LOI	0.14	3.09	n.d.	7.20	5.52	n.d.
Total	96.52	83.48	n.d.	66.70	70.30	n.d.
CO_2	n.d.	n.d.	n.d.	0.44	0.22	n.d.
S	n.d.	n.d.	n.d.	0.13	0.10	n.d.
F	n.d.	n.d.	n.d.	23.80	25.30	n.d.
Ti	1366	1941	n.d.	n.d.	n.d.	n.d.
V	58	33	n.d.	n.d.	n.d.	n.d.
Cr	8.1	6.2	n.d.	n.d.	n.d.	n.d.
Mn	248	436	n.d.	n.d.	n.d.	n.d.
Co	1.98	2.5	n.d.	n.d.	n.d.	n.d.
Ni	3.4	3.4	n.d.	n.d.	n.d.	n.d.
Cu	19	9.2	n.d.	n.d.	n.d.	n.d.
Zn	66	102	n.d.	n.d.	n.d.	n.d.
Rb	126	102	n.d.	n.d.	n.d.	n.d.
Sr	87	194	n.d.	n.d.	n.d.	n.d.
Y	22	113	98	101	90	117
Zr	203	132	n.d.	n.d.	n.d.	n.d.
Nb	33	20	n.d.	n.d.	n.d.	n.d.
Mo	3.5	3.2	n.d.	n.d.	n.d.	n.d.
Cs	1.08	1.04	n.d.	n.d.	n.d.	n.d.
Ba	156	185	n.d.	n.d.	n.d.	n.d.
La	3182	23,216	4110	79,375	49,581	74,118
Ce	4268	29,649	5752	92,161	55,749	68,830
Pr	369	2484	473	6474	3958	5240
Nd	945	6261	1225	15,000	9380	12,740
Sm	56	327	77	1434	963	1288
Eu	9	48	12	164	114	146
Gd	37	232	23	282	203	252
Tb	2.2	11.3	2.04	21.7	19.6	20.5
Dy	5.6	23	6.42	67.8	65	66
Ho	0.84	3.3	0.94	8.7	7.12	7.65
Er	2.2	9	2.38	15.2	14.1	14.5
Tm	0.3	1	0.3	1.31	1.2	1.29
Yb	2	5.9	1.25	5.5	6	6.87
Lu	0.29	0.8	0.14	0.43	0.61	0.64
Hf	7.2	3.8	n.d.	n.d.	n.d.	n.d.
Ta	1.24	0.9	n.d.	n.d.	n.d.	n.d.
Pb	112	63	n.d.	n.d.	n.d.	n.d.
Th	47	239	n.d.	n.d.	n.d.	n.d.
U	15.9	9.8	n.d.	n.d.	n.d.	n.d.

Note. The content of the oxides is given in weight %, of the elements in ppm. 1, 2, mineralized breccias; 3–6, vein-like bodies; n.d., not determined.

Fluorite is represented by two generations. The first of them composes phenocrysts up to 0.5–1.5 cm in size among the fine-grained aggregate of the bulk fluorite. It does not contain inclusions of other minerals, only occasionally there are single grains of phlogopite. The outer 1–2 mm wide edge of the grains has a dark purple (up to black) color, most likely due to radiation from thorium-containing monazite.

The bulk of fluorite (second generation) is represented by isometric and irregularly shaped grains up to 2–3 mm in size. Bastnaesite-(Ce), monazite-(Ce), and phlogopite associate with the mineral. This mineral, like the early generation, has a dark purple color. Crushed portions of the fluorite are cemented by aggregates of plumbojarosite.

In the host rocks, uneven-grained branching hydrothermal streaks of fluorite are sometimes found.

Fluorine-phlogopite in the bastnaesite and fluorite rocks composes a relatively uniform impregnation, and at the contact of the bodies, it creates scale aggregates. Its grains are often deformed, split and disintegrated. This mineral is often represented by large (more than 1 cm) crystals, schlieren-like clusters in the bastnaesite-(Ce). It composes at the contacts of bastnaesite and fluorite bodies zones abundant with monominerals. Its composition lies in the field of tetraferriphlogopite (Fig. 6, Table 3). The value of ferruginosity (F_m) varies between 17 and 31%. Manganese was found in most samples up to tenths of a percent. The mineral does not contain water, and the OH–F position is completely filled with fluorine (up to 8 wt.%). In fluorine-phlogopite, present as inclusions in phenocrysts of bastnaesite-(Ce), there is the highest concentrations of magnesium (22–23 wt.% of MgO), the MgO content varies in later generations of this mineral, between 17–19 wt.%.

Phlogopite of calcite associations in contrast to the fluorite-bastnaesite mineral paragenesis is characterized by lower concentrations of magnesium, fluorine, and high aluminum, iron and titanium (Table 3, ans. 7–12). According to its composition, the muscovite from the calcite associations corresponds to the intermediate member of the muscovite-aluminum-celadonite series, it contains iron (up to 5.8 wt.% of FeO) and magnesium (up to 1.7 weight of MgO) (Table 3, ans. 13–15).

Monazite-(Ce) was found in small amounts in fluorite-bastnaesite, calcite and albite-calcite associations. In all cases, it is represented by a scattered impregnation of tabular and irregular-shaped grains, distanced from the bastnaesite-(Ce). In large quantities, it is present in the calcite rocks (Fig. 5). This mineral from the fluorite-bastnaesite paragenesis contains up to 4 wt.% thorium (Table 2), which caused an increased radioactivity of the rocks (25–50 μR/h) and the dark purple (to black) color of fluorite.

There is no thorium in the monazite-(Ce) from the calcite association, but we have found a few percent of sulfur (Table 2). The ratios of light lanthanides in the monazites are noticeably different from the ratios in bastnaesites due to a higher neodymium content (Table 2, ans. 20–25).

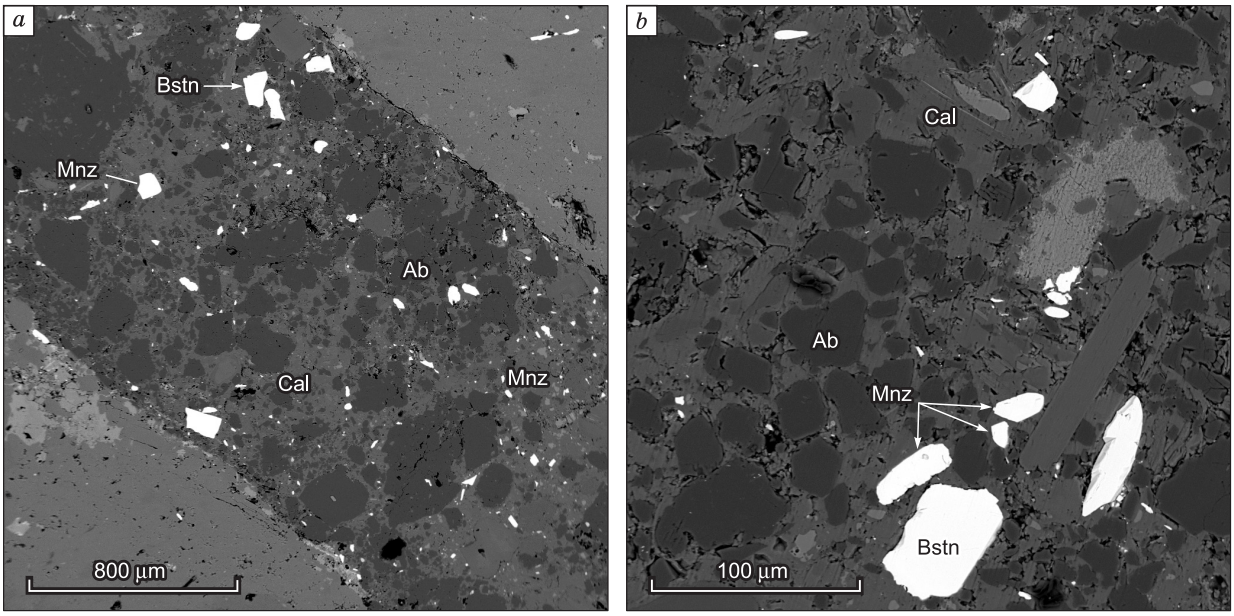

Fig. 5. The composition and structural features of the albite-calcite rocks. The rock contains bastnaesite (Bstn) (separate grains) and monazite (Mnz). Calcite (Cal) and associated rare-earth minerals occupy the interstices within albite (Ab).

The sulfates belong to characteristic minerals of the fluorite-bastnaesite rocks. Glauberite, jarosite, plumbojarosite, barite, and corkite were found in the rocks. Glauberite and plumbojarosite were found in the bastnaesite-(Ce) phenocryst in the form of a teardrop-shaped segregations and inclusions of well-formed crystals and microgranular aggregates (Fig. 7*a*, *b*, *c*). A late plumbojarosite generation is represented by fine-grained aggregates in fluorite-bastnaesite matrix that cements areas of crushed grains of phlogopite, bastnaesite-(Ce), fluorite (Fig. 7*d*, *e*, *f*), it composes the margins around the bastnaesite-(Ce) grains. In association with the plumbojarosite, we have found corkite grains with irregular shapes. The mineral compositions are presented in Table 4.

A glauberite feature is the presence of potassium, chlorine, increased amounts of fluorine and strontium. Plumbojarosites are characterized by a high heterogeneity of compositions. The iron content varies in it (between 18 and 43 wt.% of Fe_2O_3) and lead (between 5.5 and 21 wt.% PbO). The early generation is characterized by higher potassium content in general. Potassium and phosphorus are detected in the jarosites.

Zircon is represented by small irregularly shaped grains in bastnaesite of the early generation (Fig. 4*a*). Single grains of zircon are detected in micaceous aggregates of contact zones of the fluorite-bastnaesite rocks. No impurity elements were found in the mineral composition.

Ilmenite was found in the form of tabular grains in bastnaesite-(Ce) and albite (Fig. 4*a*). It is characterized by high concentrations of manganese, ranging between 7 and 16 wt.% of MnO, allowing it to be a manganilmenite. This mineral has inclusions of ferropseudobrookite, niobium-bearing rutile and titanium-containing magnetite.

Apatite is an accessory mineral. It is detected in the form of inclusions in monazite-(Ce), found in the calcite rocks. This mineral belongs to fluorapatites (4–5 wt.% of F). The impurity content is beyond the sensitivity of the analysis method.

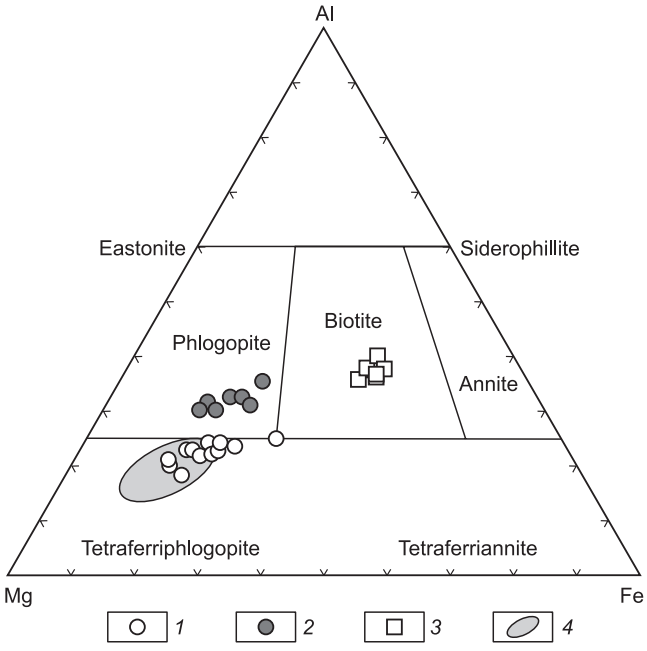

Fig. 6. The diagram of compositions of iron-magnesia mica from the fluorite-bastnaesite (*1*), albite-calcite (*2*) and enclosing crystalline schists (*3*). Shaded field (*4*)—mica from the carbonatites of the South Western Transbaikalia (Ripp et al., 2000). The diagram was taken from (Brod et al., 2001).

Table 2. The bastnaesite-(Ce) and monazite-(Ce) compositions from the bastnaesite-fluorite and calcite-containing associations, wt.%

No.	Sample	Ce_2O_3	La_2O_3	Pr_2O_3	Nd_2O_3	ThO_2	P_2O_5	SO_3	F	Total	Ce/La	Ce/Nd	La/Nd
Bastnaesite-fluorite rocks													
Bastnaesite-(Ce) of the early stage													
1	1-1/6	34.87	33.53	2.08	4.40	–	–	–	6.71	81.59	1.04	7.93	7.62
2	1-2/1	37.83	31.27	1.79	5.79	–	–	–	6.7	83.37	1.21	6.53	5.40
3	1-2/2	34.25	31.98	2.18	6.22	–	–	–	6.01	80.63	1.07	5.51	5.14
4	1-2/4	37.84	27.82	1.88	6.63	–	–	–	7.29	81.46	1.36	5.71	4.20
Average (8)		35.85	31.26	1.98	5.48	-	–	–	6.82	–	–	–	–
Bastnaesite-(Ce) of the late stage													
5	3/2	37.52	25.81	2.47	7.44	–	–	–	6.39	79.63	1.45	5.04	3.47
6	3/3	37.19	29.85	2.32	5.73	–	–	–	6.71	81.79	1.25	6.49	5.21
7	3/4	37.33	25.59	1.88	8.01	–	–	–	6.23	79.05	1.46	4.66	3.19
8	3/5	35.96	27.98	2.19	5.83	–	–	–	6.83	78.79	1.29	6.17	4.80
9	1-2/5	36.87	24.55	2.7	8.63	–	–	–	6.45	79.20	1.50	4.27	2.84
10	1-3/1	38.28	27.83	2.74	6.99	–	–	–	6.74	82.57	1.38	5.48	3.98
11	1-4/1	37.49	28.57	2.08	6.73	–	–	–	5.98	80.86	1.31	5.57	4.25
12	1-5/1	36.53	27.68	1.85	6.28	–	–	–	6.11	78.44	1.32	5.82	4.41
Average (11)		37.21	27.09	1.95	6.94	–	–	–	6.42	–	–	–	–
Monazite-(Ce)													
13	1-1/4	35.62	20.75	2.64	9.48	1.55	28.99	–	–	100.09	1.72	3.76	2.19
14	1-5/7	36.18	19.66	1.95	7.72	2.96	27.13	–	–	97.04	1.84	4.69	2.55
15	1-1/5	35.62	20.75	2.64	9.48	1.55	28.99	–	–	100.09	1.72	3.76	2.19
Average (5)		36.09	21.63	2.27	8.07	2.02	28.54	–	–	–	–	–	–
Albite-calcite rocks													
Bastnaesite-(Ce)													
16	3/5	35.4	26.9	1.97	6.75	–	–	–	8.3	79.33	1.31	5.24	3.98
17	4/5	37.93	25.57	2.26	7.23	–	–	–	7.69	80.67	1.48	5.24	3.53
18	6/5	35.95	26.19	1.57	6.82	–	–	–	8.15	79.17	1.37	5.27	3.84
19	7/5	35.57	28.45	1.40	5.61	–	–	–	8.05	75.09	1.25	6.34	5.07
Average (4)		36.21	26.77	1.80	6.61	–	–	–	8.04	–	–	–	–
Monazite-(Ce)													
20	5/1	35.22	22.06	2.16	8.17	–	30.22	–	–	96.48	1.59	4.31	2.7
21	5/2	32.47	22.86	2.57	7.45	–	29.35	1.07	–	96.48	1.55	4.76	3.06
22	5/2-3	34.12	24.23	1.78	6.49	–	29.54	–	–	98.03	1.41	5.25	3.73
23	6/1	34.44	23.22	1.92	6.95	–	28.04	0.95	–	96.17	1.48	4.95	3.34
24	6/1-2	33.04	26.29	1.40	6.46	–	29.42	–	–	97.09	1.25	5.11	4.06
25	7/3	30.96	20.29	1.31	5.77	–	28.89	2.12	–	91.96	1.52	5.36	3.51
Average (6)		33.87	23.15	1.85	6.88	–	29.24	–	–	–	–	–	–

GEOCHEMICAL FEATURES OF BASTNAESITE AND FLUORITE ROCKS

The distribution heterogeneity of the composing minerals and xenoliths present in host rocks determined the heterogeneity of the rock composition. In mineralized breccias, the REE contents range between 1–2 and 5–6 wt.% of oxides, in massive fluorite-bastnaesite bodies, the total REE contents vary between 15–20 and 31 wt.% of oxides (Table 1). Light lanthanides predominate in the composition of rare-earth elements in the bastnaesite-fluorite rocks, the main part of which is concentrated in bastnaesite, with an average La/Yb ratio of 7000. On the chondrite-normalized REE spectra (Fig. 8) the rocks form an inclined curve with the lack of an europium anomaly. The highest concentrations of REE are typical for the brecciated bastnaesite and fluorite rocks of the Smolin site. The rocks of the Ulan-Ude and Portovyi occurrences on these graphs have a similar curve, but they are characterized by lower content of light lanthanides. The configuration of REE graphs is similar to that of the late Mesozoic carbonatites in Western Transbaikalia (Fig. 8).

Table 3. The compositions of iron-magnesian micas from the enclosing, bastnaesite and calcite-containing rocks, wt.%

No.	Sample No.	SiO_2	TiO_2	Al_2O_3	FeO	MnO	MgO	K_2O	F	Total	$0 = F_2$	F_m
Bastnaesite-fluorite rocks												
Initial stage												
1	1-3/6	40.54	1.63	10.30	17.92	0.63	14.96	11.12	3.11	100.21	1.31	40.20
2	1-5/2	42.74	1.08	9.20	11.90	0.36	17.31	11.19	5.00	98.80	2.11	27.80
3	1-5/5	42.34	1.00	8.82	9.51	0.35	18.56	11.46	4.38	96.41	1.85	22.30
Average (7)		42.29	1.35	9.46	12.66	0.44	17.42	11.35	4.11	–	–	–
Main stage												
4	3-2/2	42.47	1.2	8.69	9.94	0.48	17.96	11.37	4.77	97.34	2.01	23.70
5	3-2/3	43.92	0.97	7.97	8.14	0.34	19.49	11.53	5.12	97.47	2.16	19.00
6	3-3/1	43	0.73	8.16	10.38	0.71	17.43	11.19	5.93	97.54	2.50	25.10
Average (8)		43.33	0.93	8.13	9.57	0.54	17.20	11.16	5.46	–	–	–
Albite-calcite rocks												
7	4/2	36.67	1.70	13.98	13.86	1.27	14.64	10.64	3.41	96.16	1.44	2.4
8	4/3	35.41	1.55	15.32	15.34	0.98	13.66	10.73	3.23	96.23	1.36	2.88
9	5/3-2	37.01	1.37	13.98	10.92	1.30	15.77	11.06	4.4	95.83	1.86	4.08
10	6/1	41.42	1.78	11.70	11.19	0.32	15.34	11.12	5.38	101.75	2.27	3.57
11	6/2	35.43	1.88	15.63	16.13	0.74	13.07	10.54	2.61	96.53	1.11	2.59
12	7/2-1	39.77	0.88	13.42	10.07	1.02	17.64	11.26	5.65	99.72	2.39	4.99
13	7/3	44.16	0.72	27.93	5.80	–	1.71	11.99	1.07	93.37	0.45	1.52
14	7/4	44.36	1.83	29.36	5.00	–	1.07	11.78	–	93.32	–	1.38
15	7/5	43.84	1.05	28.29	5.11	–	1.49	11.7	1.39	92.76	0.58	1.52
Crystalline schists												
16	2-3/6	35.09	1.88	15.95	23.45	–	8.39	10.22	–	94.98	–	61.10
17	2-3/7	35.32	1.73	16.14	23.20	–	7.76	10.55	–	94.70	–	62.70
18	2-3-1/4	38.89	2.15	16.00	21.61	–	8.51	10.12	–	97.98	–	58.80
Average (5)		35.84	1.68	16.08	23.55	–	8.19	10.33	–	–	–	–

Note. The initial stage includes zoned phenocrysts and inclusions in the bastnaesites, the main stage includes the mineral which is scattered in the fluorite matrix. Samples 13–15, muscovite.

On primitive mantle-normalized rare elements spectra the bastnaesite-fluorite rocks are characterized by negative anomalies in Nb, Ta, Pb, Zr, Hf, and Ti with respect to neighboring elements (Fig. 8). The rocks have similar distribution spectra of rare elements with those for the late Mesozoic carbonatites of Western Transbaikalia (Fig. 8). As regards to carbonatites, there are clearly expressed minima for Ba and Sr, which is due to the absence of barium and strontium sulfates (barite and barite-celestine) on the studied occurrences and their prevalence in carbonatites of Western Transbaikalia.

The isotopic value of $\delta^{13}C_{V\text{-}PDB}$ in the bastnaesite-(Ce) from the bastnaesite-fluorite rocks and the calcite varies between –5.9 and –8.3‰ and between –3.6 and –6.6‰, respectively (Fig. 9, Table 5). The data obtained lie in the field of the mantle carbonates (PIC) and are similar to the unchanged carbonates from the carbonatites of Arshan and Yuzhnoe occurrences (Ripp et al., 2000). The value of $\delta^{18}O_{V\text{-}SMOW}$ for the phlogopite makes up +1.1‰.

The primary isotopic strontium ratio in the bastnaesite (0.70559) and fluorite (0.70568) from fluorite-bastnaesite rocks are identical to those in the carbonatites of Southwestern Transbaikalia (Ripp et al., 2000).

THE RESULTS OF STUDY OF FLUID INCLUSIONS IN MINERALS

Three types of fluid inclusions were detected in the fluorite and bastnaesite of the Ulan-Ude occurrence at room temperature (Fig. 10). The first group is represented by highly concentrated brine and melt inclusions (Fig. 10*a*, *b*), which are arranged individually or in groups of 2–3 inclusions in the central areas of the crystals of the early bastnaesite and fluorite. The shape of the vacuole of brine and melt inclusions is round, isometric, often presented as negative forms of a crystal. Sometimes, the groups of brine and melt inclusions are located in the growth zones of fluorite crystals, which confirms the primary capture of inclusions.

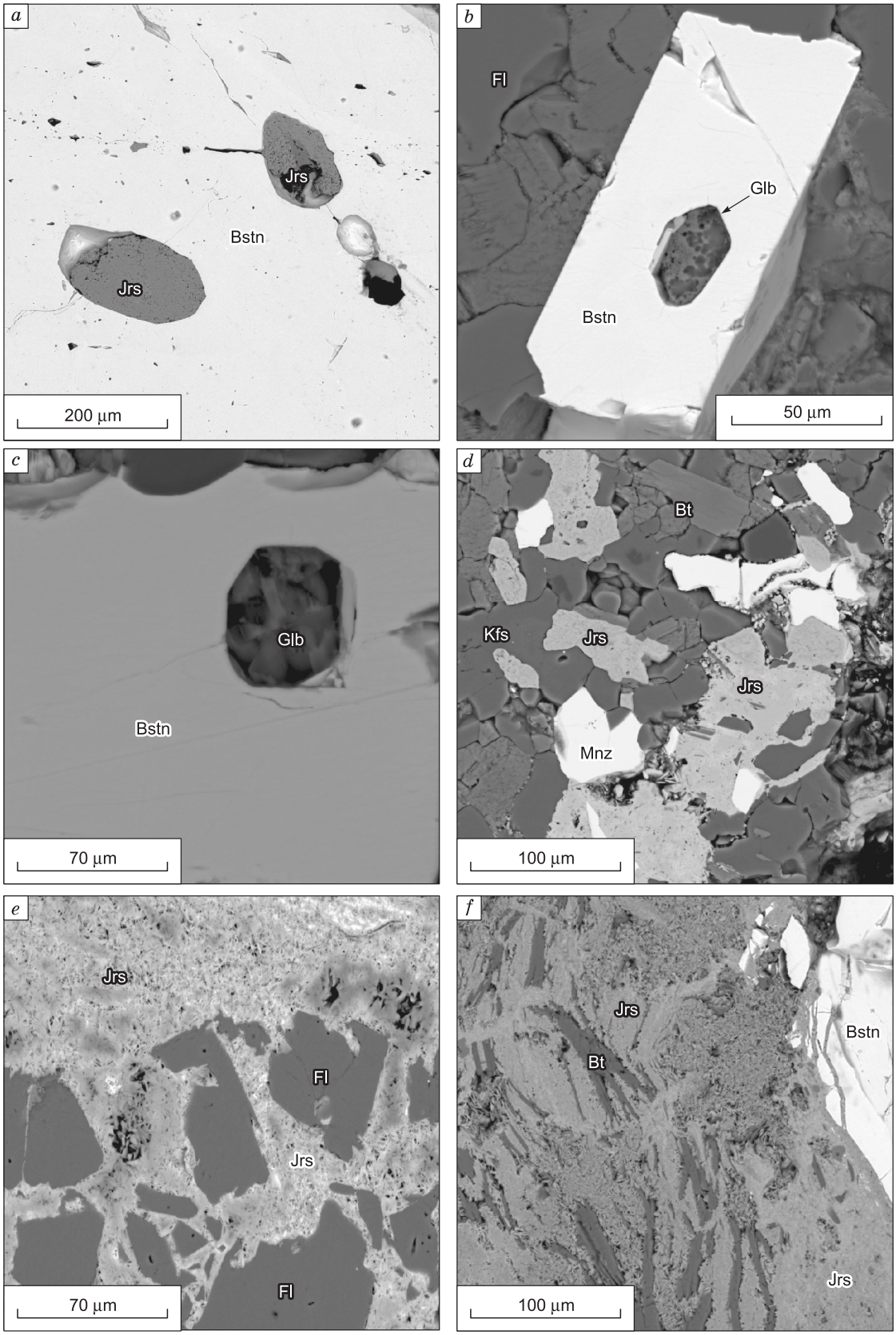

Fig. 7. The character of sulfate minerals nodules in the fluorite-bastnaesite rocks. *a–c*, the inclusion of an early glauberite (Glb) and a plumbojarosite (Yrs) in association with monazite (Mnz); *d–f*, a late plumbojarosite generation cementing the crushed parts of fluorite (*e*) and bastnaesite, phlogopite (*c*).

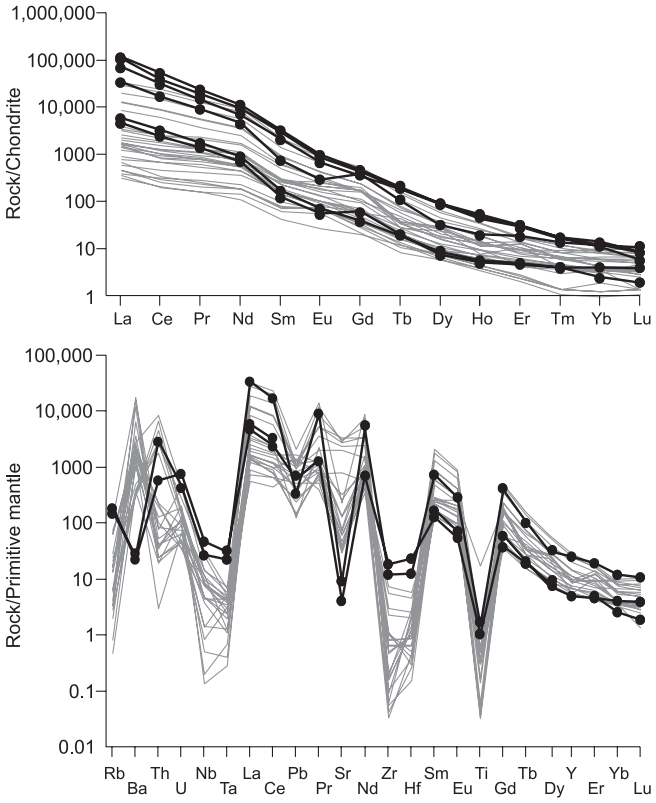

Fig. 8. The distribution of rare-earth elements normalized to the chondrite (McDonough and Sun, 1995) and rare elements normalized to primitive mantle (Sun and McDonough, 1989) in the fluorite-bastnaesite rocks of the Ulan-Ude occurrence. Gray lines—late Mesozoic carbonatites of Western Transbaikalia (Arshan, Yuzhnoe, Khalyuta) by (Ripp et al., 2000; Doroshkevich, 2013).

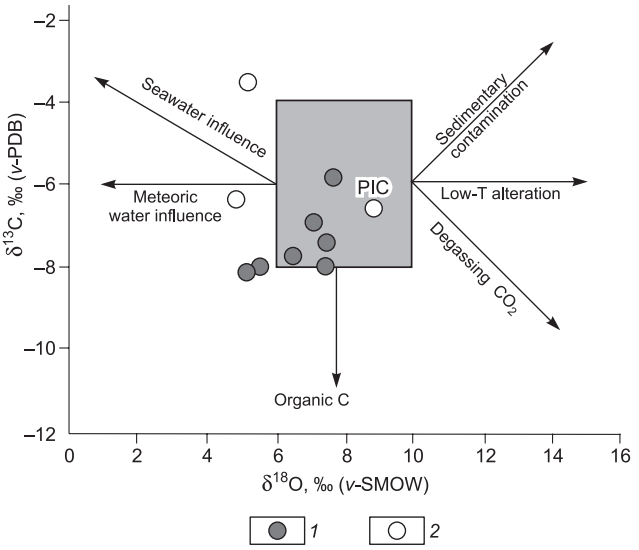

Fig. 9. The diagram with the isotopic composition of oxygen and carbon in the bastnaesite (*1*) and the calcite (*2*) of the Ulan-Ude occurrence. The PIC area and the changing trends in the isotopic compositions of O and C according to (Demény et al., 2004).

Highly concentrated brine-melt inclusions consist of the mineral, liquid and gas phases. The mineral phase, the amount of which reaches 80–90 vol.% is represented by an aggregate of closely contiguous grains of irregular, rectangular, elongated, isometric shapes. The gas bubble is often deformed, and its shape is determined by the free space. The amount of the gas phase is in the range of 5–10 vol.%. The rest of the space is occupied by liquid. The size of brine and melt inclusions can reach 50 microns, and an average of 15–20 microns.

The second type of inclusions is represented by multiphase crystal-fluid inclusions (Fig. 10*c*, *d*). The fluid inclusions are pseudosecondary, as they are located in groups along healed fractures in the crystals of bastnaesite and fluorite of the first generation. In addition, the inclusions are primary with respect to the late generation of matrix minerals. The shape of the inclusions' vacuole is round, isometric, rarely elongated and has the form of negative crystals, the size of the inclusions averages 10–15 microns. The inclusions contain solid, liquid and gas phases. The amount of mineral phase makes up 30–50 vol.%. The solid phase forms crystals of cubic, rectangular and isometric shapes. The gas bubble takes up to 10–20 vol.%.

The third type of inclusions are secondary and pseudosecondary gas-liquid water-salt inclusions (Fig. 10*e*, *f*), which may also contain one or two crystalline phases (up to 5–10 vol.%). These inclusions are located along cracks and surfaces, and form plumes, sometimes with traces of pinching. The vacuole shape of the inclusions usually is elongated, rarely isometric, irregular, and their size does not exceed 15 microns. These are gas-liquid inclusions of various generations, where a gas bubble takes from 10 to 90 vol.%, and the rest of the space is occupied by liquid.

The results of the diagnostics of the subsidiary crystalline phases brine and melt inclusions have established the predominance of Na and Ca sulphates, glauberite and thenardite, in the composition of the inclusions (Fig. 11*a*). In addition to sulfates, there are phases of aluminosilicate minerals in brine and melt inclusions—phlogopite (?), carbonates and rare-earth phases – calcite, parisite (?), the latter is also noted in the composition of crystal-fluid inclusions (Fig. 11*b*, *c*). According to Raman scattering spectroscopy, the gas phase of brine and melt inclusions contains liquid carbon dioxide. The content of salt components of brine and melt inclusions can be estimated at 80–90 vol.%, with sulfates in volume by almost half dominated by the carbonate and silicate phases. The total concentration of salts in the inclusions exceeds 80 wt.% (Table 6). The homogenization temperatures of brine and melt inclusions of small sizes are in the range of 490–520 °C. The heating process of the smallest brine and melt inclusions occurred with the gradual dissolution of the daughter crystalline phases forming the liquid phase, followed by the disappearance of the gas phase and the formation of a homogeneous melt in the inclusion. When cooling, the inclusions returned to the initial phase state.

Table 4. The chemical compositions of the sulfate minerals from bastnaesite-fluorite rocks, wt.%

No.	FeO	CaO	Na_2O	K_2O	SrO	PbO	P_2O_5	SO_3	Cl	F	Total
Glauberite											
1	–	20.90	17.07	–	2.39	–	–	51.14	1.07	3.25	95.82
2	–	21.44	17.73	0.29	1.81	–	–	57.55	1.00	2.00	94.81
3	–	22.81	14.80	0.25	1.96	–	–	51.69	1.22	3.00	95.74
4	–	21.39	16.01	0.28	1.18	–	–	50.55	0.81	1.61	91.83
5	–	19.88	19.88	0.20	1.97	–	–	47.01	0.55	3.57	93.06
6	–	21.23	17.84	0.22	0.55	–	–	50.27	1.26	3.47	94.84
7	–	22.00	19.85	0.45	1.71	–	–	54.21	н/о	н/о	98.32
Jarosite											
8	40.64	–	–	7.67	–	–	–	30.52	–	–	83.59
9	36.25	–	–	6.49	–	–	–	27.22	–	–	77.18
Plumbojarosite-I											
10	38.90	–	–	6.40	–	11.04	–	28.24	–	–	84.58
11	40.19	–	–	7.28	–	7.82	–	29.84	–	–	85.13
12	36.54	–	–	5.61	–	14.76	–	26.67	–	–	85.58
13	37.62	–	–	5.95	–	14.62	1.54	25.32	–	–	85.04
14	35.20	–	–	4.95	–	16.60	1.54	27.67	–	–	82.56
15	38.10	–	–	6.00	–	11.48	0.73	26.92	–	–	83.13
16	35.66	–	–	6.08	–	10.97	1.21	24.40	–	–	78.32
Plumbojarosite-II											
17	36.24	–	–	4.18	–	19.19	2.52	22.27	–	–	84.40
18	35.56	–	–	3.40	–	21.30	3.96	18.83	–	–	82.76
19	42.75	–	–	4.88	–	10.85	–	21.58	–	–	80.05
20	39.75	–	–	7.52	–	5.53	–	28.99	–	–	81.86
21	37.33	–	–	4.94	–	15.80	0.92	24.92	–	–	84.11
22	38.59	–	–	5.83	–	12.15	0.69	27.34	–	–	84.61
23	39.80	–	–	2.29	–	21.32	3.09	17.85	–	–	84.35
24	38.02	–	–	4.95	–	16.04	0.66	25.90	–	–	85.57
25	42.47	–	–	8.41	–	6.20	–	31.31	–	–	88.39
26	39.70	–	–	3.70	–	14.42	1.17	20.68	–	–	79.67
Corkit											
27	–	–	–	0.55	–	28.24	7.33	13.09	–	–	77.81
28	–	–	–	1.73	–	26.89	6.12	16.81	–	–	81.75

The diagnosis of the composition of crystal-fluid inclusions containing up to 30–50 vol.% of salt phases showed the presence of carbonates and Ca and Na sulfates and REE carbonates. The temperature range of homogenization of salt fluid solutions is 430–450 °C (Table 6). The total concentration of salts in inclusions by volume ratios can be estimated at 40–60 wt.%. In the fluorite of late generations, we detected primary-secondary fluids containing single isotropic crystals of cubic form—the Na and/or K chlorides responsible for the secondary processes of mineral formation. The homogenization temperatures of chloride fluid inclusions correspond to the range of 290–350 °C, the gas phase of crystal-fluid inclusions contains CO_2. The melting temperature of the daughter phases in thermometry give estimates of the concentration of fluid solutions in 30–15 wt.% NaCl-equiv. (Table 6).

The gas-liquid secondary fluid solutions in bastnaesite and fluorite are homogenized at temperatures of 150–200 °C. The inclusions contain crystals of Ca, Mg and Fe hydrosulfates, Ca and Na hydrocarbonates, and the gas phase consists of $CO_2 \pm H_2$ (Table 6). The late abundant with gases fluid inclusions (Fig. 10*f*) in the fluorite may also indicate the boiling of fluids in the process of late transformations of the hydrothermal system.

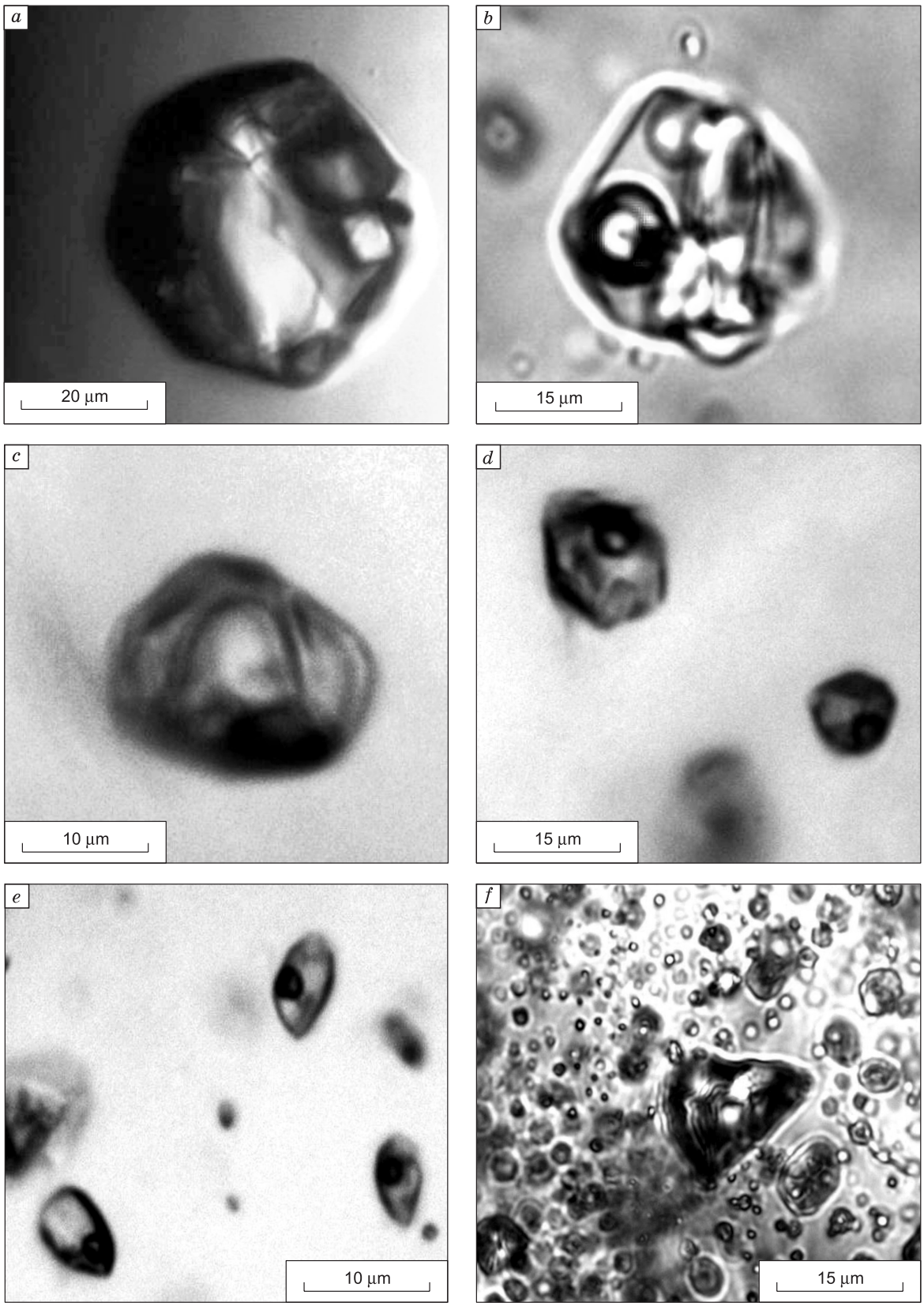

Fig. 10. The inclusions in minerals from the rocks of the Ulan-Ude occurrence. The salt brined and melt inclusions in bastnaesite (*a*) fluorite and (*b*); of crystal-fluid inclusions in bastnaesite (*c*, *d*); gas-liquid inclusions in bastnaesite (*e*) and fluorite (*f*).

Table 5. The isotopic characteristic of minerals from the bastnaesite and fluorite and calcite-containing rocks

Sample	Mineral	$\delta^{13}C‰_{V\text{-}PDB}$	$\delta^{18}O‰_{V\text{-}SMOW}$	$(^{87}Sr/^{86}Sr)_0$
Bastnaesite-fluorite rocks				
U-U-1	Fluorite			0.70568 ± 10
U-U-2	Bastnaesite-(Ce)	–8.1	+7.4	0.70559 ± 9
P-1	Bastnaesite-(Ce)	–5.9	+4.8	–
SM-18-1	Bastnaesite-(Ce)	–8.3	+5.5	–
SM-18-2	Bastnaesite-(Ce)	–7.8	+4.3	–
SM-18-2a	Bastnaesite-(Ce)	–8.3	+5.4	–
B-15-1	Phlogopite		+1.1	–
B-15-1б	Phlogopite		+1.1	–
B-15-2	Phlogopite		+2.3	–
SM-17-1	Phlogopite		+1.2	–
SM-17-2	Phlogopite		+0.3	–
Albite-calcite rocks				
SM-4-18	Calcite	–6.5	+8.3	–
SM-4-18a	Calcite	–6.1	+4.6	–
SM-10-18	Calcite	–3.6	+5.4	–
SM-5-18	Calcite	–6.6	+7.9	–

Table 6. The results of thermobarogeochemical studies of the inclusions in minerals of Ulan-Ude occurrence

Type of fluid inclusions	Matrix	T_{hom}, °C	Composition/concentration, wt.%	The composition of the crystal phases (scattering spectroscopy, Raman)
Brined-melted, primary	Bastnaesite, fluorite	490–520	Ca^{2+}, Na^+, SO_4^{2+}, REE, CO_2 (Liquid) – H_2O/> 80	Glauberite, thenardite, phlogopite (?), calcite, parisite (?)
Crystal-fluid, pseudosecondary	Bastnaesite, fluorite	430–450	Ca^{2+}, Na^+, SO_4^{2+}, REE, CO_2 – H_2O/40–60	Thenardite, glauberite, parisite (?)
Water-salt, primarysecondary	Fluorite	290–350	NaCl/KCl – H_2O, CO_2 (Gas)/30–15 NaCl-equiv.	Halite/Sylvite
Gas-liquid, secondary	Bastnaesite, fluorite	150–200	Ca^{2+}, Na^+, Mg^{2+}, Fe^{3+}, HSO_4^+, HCO_3^+, $CO_2 \pm H_2$ – H_2O/1–10	Ca, Mg and hydrosulfates Fe, Hydrocarbonates of Ca and Na

DISCUSSION

The bastnaesite-containing deposits that are known to exist are associated mainly with carbonatites and alkaline rocks associated with them. For the discussed case, it is important that in the 26 to 40 km to the south from the described occurrence, there are several, including bastnaesite-containing (Arshan, Yuzhnoe) occurrences of carbonatites. The proximity of ages (135–122 Ma (Ripp et al., 2000)), mineralogical and geochemical features with the studied occurrence suggests with a high degree of confidence a genetic relationship with the late Mesozoic carbonatites of the southwestern Transbaikalia. This is also evidenced by the values of Sr_0 in bastnaesite and fluorite, the curves of normalized REE contents, the compositions of carbon and oxygen in the carbonates. The latter lie, as in the case of carbonatites, in the boundaries of the PIC field (Ripp et al., 2000; Doroshkevich, 2013). Like the carbonatites, magnesia and fluorine contents are increased in the micas of the studied occurrences, and their composition corresponds to tetraferriphlogopite (Fig. 5).

The parageneses with fluorite and rare-earth mineralization are often detected in many occurrences of carbonatites in the world. They are described in the following deposits: Kangankunde (Wall et al.,1994), Karasug (Nikiforov et al., 2005), Amba–Dongar (Doroshkevich et al., 2009), Barra do Itapirapua (Ruberti et al., 2008), Bayan Obo (Tao et al., 1996), and they are often identified as hydrothermalites (Williams-Jones et al., 2000; Anderson et al., 2013; Liu et al., 2018) or as carbothermal formations (Mitchell, 2005). In the bastnaesite- and fluorite-bearing carbonatites of the Yuzhnoe and Arshan districts, located at 26–40 km from the described occurrences, the processes of silicification, of replacement of bastnaesite with parisite, ancylite and allanite are detected at the post-carbonatite stage (Ripp et al., 2000, Doroshkevich et al., 2008). Therefore, the arguments of high-temperature formation of the studied rocks include as follows: structural-textural features of rocks (equigranular

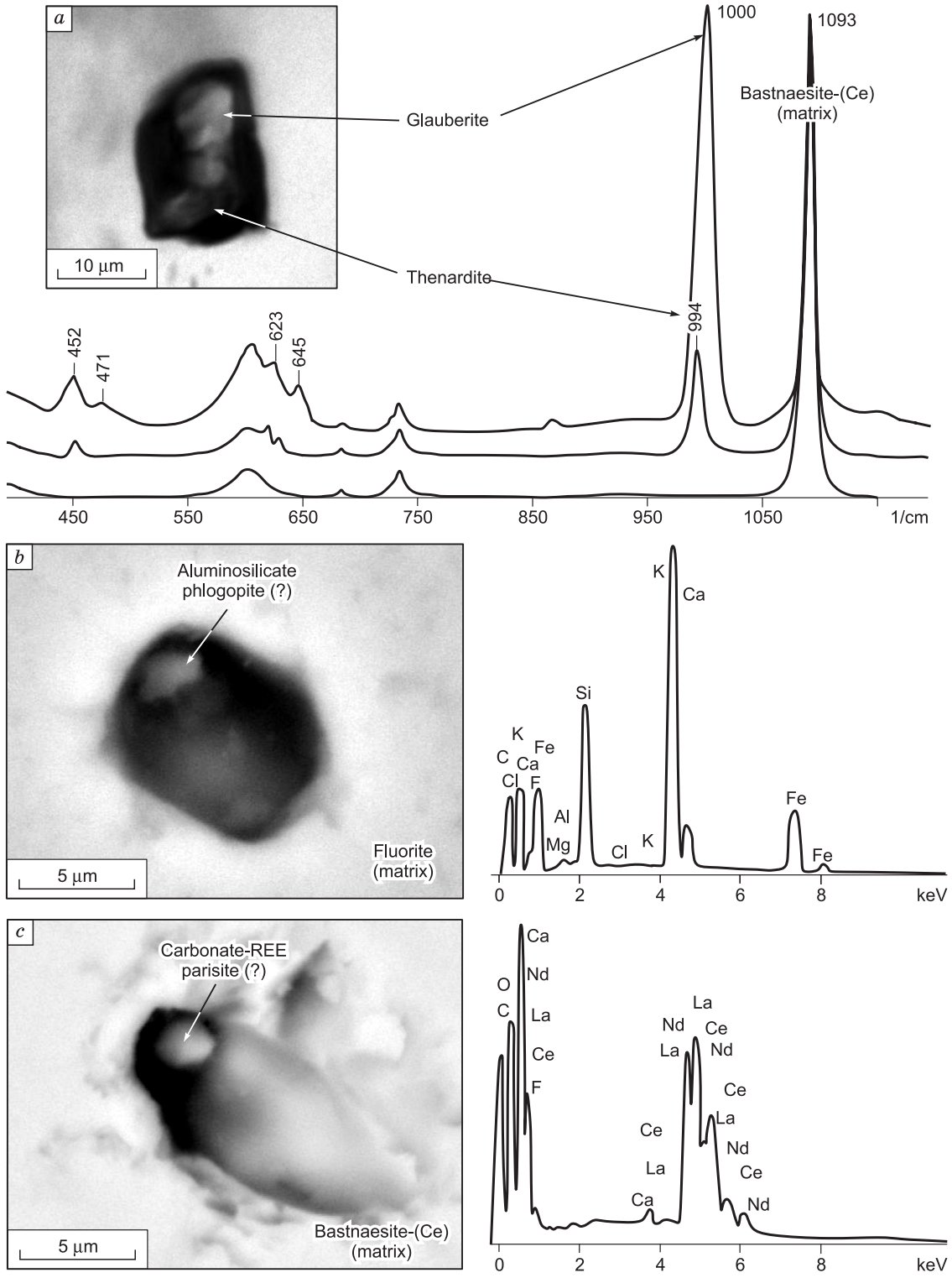

Fig. 11. Study results of inclusions compositions in the minerals from the rocks of the Ulan-Ude occurrence: *a*, Raman spectra of the daughter crystalline phases glauberite and the thenardite of the brine and melt inclusion from bastnaesite (photo); *b*, *c*, the diagnostic results of the crystalline phases in the exposed particles using scanning electron microscopy (photo and spectrum of the studied phases): aluminosilicate phase—phlogopite (?) in the brined and melted inclusion in fluorite (*b*) and carbonate-REE—parisite (?) in the crystal-fluid inclusion in bastnaesite (phase spectra contain elements of the matrix of inclusions).

texture, the presence of phenocrysts, traces of flow with the presence of gas voids), which is more likely coincident with magmatic way of their formation; the boundaries of the xenoliths (despite the varied composition) with fluorite-bastnaesite units are sharp, with no reaction rims; high temperatures of homogenization of primary inclusions in bastnaesite (490–520 °C).

The fluid mode of formation of carbonatites in the Western Transbaikalia has been studied relatively poorly. Up to the present time, only the estimates of the hydrothermal (330–210 °C) mineralization of the carbonatites (Bulnaev, 1985, 2000) have been made. The first crystal-fluid inclusions were established and studied at the Yuzhnoe and Arshan REE-carbonatites (Doroshkevich and Ripp, 2004). It was found that the bastnaesite of carbonatites was formed at temperatures above 520 °C. It was not possible to obtain the true homogenization temperatures of brine and melt inclusions at that time due to the decomposition of the host mineral (bastnaesite) at high temperatures between 480 and 520 °C. However, it was possible to establish the presence of salt daughter phases of Na, K and Ca sulfates and fluorine-containing minerals in the inclusions (Doroshkevich and Ripp, 2004). The temperature of fluorite formation at the Arshan and Yuzhnoe deposits is in the range of 370–400 °C, and the first estimates of mineral formation temperatures at the Ulan-Ude occurrence makes up 233–237 °C (Ripp et al., 2018).

The new obtained data of investigations of the inclusions in bastnaesite and fluorite Ulan-Ude occurrence showed that rocks were formed from orthomagmatic salt brine of the carbonate (Ca, REE) and sulphate (Ca, Na) composition at temperatures above 490–520 °C. The further evolution of the orthocarbonate fluids to the hydrothermal stage took place according to the following scheme changes the technical features' conditions of the processes of mineral formation: at 450–430 °C carbonate-sulfate (30–40 wt.%) solution (Ca, Na, REE)-CO_2 → at 350–290 °C in chloride (K, Na)-CO_2 (30–10 wt.%) solution → 350–290 > 200–150 °C hydrocarbonate-sulphate–hydrocarbonate-chloride (Ca, Mg, Fe^{3+}, Na, K)-$CO_2 \pm H_2$ low-concentrated (10–1 wt.%) solution. During the first orthomagmatic stage, the main paragenesis of rocks—bastnaesite, fluorite, phlogopite, zircon, ilmenite was crystallized. At the same time, the sulfates were also changing consistently their composition from the early orthomagmatic stage (glauberite) to the hydrothermal phases (barite, crochet, and jarosite) and changing the fluid composition on low-concentrated hydrocarbonate-sulfate-chloride content.

All of the above allows us to refer the studied fluorite-bastnaesite rocks to the derivatives of the regional carbonatite ore-magmatic system, widely manifested in the form of carbonatite F–Ba–Sr and REE complexes in Western Transbaikalia: Khalyuta, Yuzhnoe, Arshan, Torei, Oshurkovo. The rock features include the presence of the sulfate minerals. They formed, starting with the initial stages (in the form of inclusions in phenocrysts) to the final, cementing the crushed portions of the previously formed fluorite, and bastnaesite, phlogopite. It should be noted that the sulfates belong to the typomorphic minerals in carbonatites of Western Transbaikalia (Doroshkevich et al., 2003). The sulfate phase, according to (Migdisov and Williams-Jones, 2014), could be one of the important transport ligands (and thus concentration) of rare-earth elements. This extends the area of distribution of such rocks and is important for deciphering the geological processes of the region and also significantly increases the prospects of rare-earth mineralization of the researched area.

Experimental studies of the carbonatite systems show that hydrothermal rare-earth minerals are typically accumulated in a solution and are crystallized as their own mineral phases as a result of fluid redistribution of the rare-earth elements in REE-containing magmatic mineral phases (Harlov et al., 2002, 2005; Harlov and Förster, 2003; Shironosova and Prokopyev, 2017, 2018). The fluids involved in the transport and crystallization of REE minerals have a high activity of anionic ligands (F, Cl, CO_2 (W), SO_4^{2-}), and are also brines in composition (Tropper et al., 2011, 2013; Williams-Jones et al., 2012). According to (Li and Zhou, 2015), the hydrothermal REE redistribution is also highly dependent on Ca and Na cationic ligands. These observations were confirmed by studies of fluid and melt inclusions in the minerals (Samson et al., 1995; Buhn and Rankin, 1999; Smith et al., 2000, 2018; Buhn et al., 2002; Xie et al., 2009; Prokopyev et al., 2016, 2017, 2018) and, of course, require close attention in the study of carbonatite complexes of Western Transbaikalia.

A certain intrigue for the studied occurrence is introduced by calcite-containing rocks. Such rocks are referred (Lapin et al., 2011) to one of the high-temperature facies (420–530 °C) of the carbonatites. The mineralogical features of these rocks allow us to speak at the present time about a probable connection with the studied occurrence. The calcite rock together with the albite was described in the Kizilcaören deposit of carbonatites (Turkey) (Nikiforov et al., 2014). This deposit is known as a large fluorite-barite rare-earth object. For our case, the nature of the calcite-containing rocks and the nature of their connection with the fluorite-bastnaesite rocks requires additional studies.

CONCLUSIONS

The performed studies allow us to draw the following conclusions. The genetic connection of the Ulan-Ude occurrence with the late Mesozoic carbonatites of the Western Transbaikalian province has been substantiated. The specificity of its composition, high concentrations of rare-earth elements were determined. Like the carbonatites of the Western Transbaikalian province, the sulfates participated in its formation. The discovery of this occurrence indicates a still insufficient geological study of the area and its high prospects for industrial rare-earth mineralization.

The geochemical studies were performed in the framework of the topics of the research activities in the Fun-

damental Scientific Research Program of the National Academy of Sciences IX.129.1.2 (state.reg. No. AAAA-A16-116122110027-2). The study of isotopic composition in the minerals was financially supported by a project of the Russian Foundation for Basic Research (No. 17-05-00129a). The study of the mineralogy of carbonatites was carried out at the expense of the Grant from the President of the Russian Federation MK-1113.2019. The thermometric experiments are funded by a grant from the Russian Science Foundation, No. 19-17-00013.

REFERENCES

Andersson, U.B., Holtstam, D., Broman, C., 2013. Additional data on the age and origin of the Bastnäs-type REE deposits, Sweden. Mineral deposit research for a high-tech world, in: Proc. 12th Biennial SGA Meeting, Uppsala, pp. 1639–1642.

Brod, J.A., Gaspar, I.C., de Araigo, D.P., Gibson, S.A., Thompson, R.N., Junqueira-Brod, T.C., 2001. Phlogopite and tetra-ferriphlogopite from Brazilian carbonatite complexes: petrogenetic constrains and implications for mineral-chemistry systematics. J. Asian Earth Sci. 19, 265–296.

Buhn, B., Rankin, A.H., 1999. Composition of natural, volatile-rich Na–Ca–REE–Sr carbonatitic fluids trapped in fluid inclusions. Geochim. Cosmochim. Acta 63, 3781–3797.

Buhn, B., Rankin, A.H., Schneider, J., Dulski, P., 2002. The nature of orthomagmatic, carbonatitic fluids precipitating REE, Sr-rich fluorite: fluid-inclusion evidence from the Okorusu fluorite deposit, Namibia. Chem. Geol. 186 (1–2), 75–98.

Bulnaev, K.B., 1985. The conditions of formation and localization of the fluorine rare-earth mineralization. Geologiya Rudnykh Mestorozhdenii XXVII (2), 28–38.

Bulnaev, K.B., 2000. Rare-earth mineralization in the linear carbonatites of the Arshan Deposit. Geologiya Rudnykh Mestorozhdenii, No. 3b, 275–280.

Coplen, T.B., 1988. Normalization of oxygen and hydrogen data. Chem. Geol. Isotope Geosci. Sect. 72 (4), 293–297.

Demény, A., Sitnikova, M.A., Karchevsky, P.I., 2004. Stable C and O isotope compositions of carbonatite complexes of the Kola Alkaline Province: phoscorite-carbonatite relationships and source compositions, in: Wall, F., Zaitsev, A.N. (Eds.), Phoscorites and Carbonatites from Mantle to Mine: The Key Example of the Kola Alkaline Province. Mineralogical Society of Great Britain and Ireland, pp. 407–431.

Doroshkevich, A.G., 2013. The Petrology of the Carbonatite and Carbonate-Containing Alkaline Complexes in the Western Transbaikalia. DrSci Thesis [in Russian]. Ulan-Ude, GI SO RAN.

Doroshkevich, A.G., Ripp, G.S., 2004. Estimation on the conditions of formation of REE-carbonatites in Western Transbaikalia. Geologiya i Geofizika (Russian Geology and Geophysics) 45 (4), 492–500 (456–463).

Doroshkevich, A.G., Kobylkina, O.V., Ripp, G.S., 2003. Role of sulfates in the formation of carbonatites in the Western Transbaikal Region. Dokl. Earth Sci. 388 (1), 131–134.

Doroshkevich, A.G., Ripp, G.S., Viladkar, S.G., Vladykin, N.V., 2008. The Arshan REE carbonatites, Southwestern Transbaikalia, Russia: minerology, paragenesis and evolution. Can. Min. 46 (4), 807–823.

Doroshkevich, A.G., Viladkar, S.G., Ripp, G.S., Burtseva, M.V., 2009. Hydrotermal REE mineralization in the Amba Dongar carbonatite complex, Gujarat, India. Can. Min. 47 (5), 1105–1116.

Fleck, R.J., Sutter, J.F., Elliot, D.H., 1977. Interpretation of discordant $^{40}Ar/^{39}Ar$ age-spectra of Mesozoic tholeiites from Antarctica. Geochim. Cosmochim. Acta 41 (1), 15–32.

Friedman, I., O'Neil, J., Cebula, G., 1982. Two new carbonate stable-isotope standards. Geostand. Newl. 6 (1), 11–12.

Harlov, D.E., Förster, H.J., 2003. Fluid-induced nucleation of (Y+REE)-phosphate minerals in apatite: Nature and experiment. Part II. Fluorapatite. Am. Mineral. 88 (8–9), 1209–1229.

Harlov, D.E., Förster, H.J., Nijland, T.G., 2002. Fluid induced nucleation of (Y+REE)-phosphate minerals in apatite: Nature and experiment. Part I. Chlorapatite. Am. Mineral. 87 (2–3), 245–261.

Harlov, D.E., Wirth, R., Förster, H.J., 2005. An experimental study of dissolution–reprecipitation in fluorapatite: fluid infiltration and the formation of monazite. Contrib. Mineral. Petrol. 150 (3), 268–286.

Lapin, A.V., Tolstov, A.V., Ploshko, V.V., Chemezova, L.N. Sorokina, T.I., 2011. The Mineralogy of Weathering Crusts of Carbonatites: Best Practice Guidance [in Russian]. GEOKART, GEOS, Moscow.

Li, X., Zhou, M.F., 2015. Multiple stages of hydrothermal REE remobilization recorded in fluorapatite in the Paleoproterozoic Yinachang Fe–Cu–(REE) deposit, Southwest China. Geochim. Cosmochim. Acta. 166, 53–73.

Liu, S., Fan, H.-R., Yang, K.-F., Hu, F-F., Wang, K.-Y., Chen, F.-K., Yang, Y.-H., Yang, Z.-F., Wang, Q.-W., 2018. Mesoproterozoic and Paleozoic hydrothermal metasomatism in the giant Bayan Obo REE–Nb–Fe deposit: Constrains from trace elements and Sr–Nd isotope of fluorite and preliminary thermodynamic calculation. Precambrian Res. 311, 228–246.

McDonough, W.F., Sun, S.-s., 1995. The Composition of the Earth. Chem. Geol. 120 (3–4), 223–253.

Migdisov, A., Williams-Jones, A.E., 2014. Hydrothermal transport and deposition of the rare earth elements by fluorine-bearing aqueous liquids. Mineralium Deposita 49 (8), 987–997.

Mitchell, R.H., 2005. Carbonatites and carbonatites and carbonatites. Can. Min. 43 (6), 2049–2068.

Nikiforov, A.A., Öztürk, H., Altuncu, S., Lebedev, V.A., 2014. Kizilcaören ore-bearing complex with carbonatites (northwestern Anatolia, Turkey): Formation time and mineralogy of rocks. Geol. Ore Deposits 56 (1), 35–60.

Nikiforov, A.V., Bolonin, A.V., Sugorakova, A.M., Popov, V.A., Lykhin, D.A., 2005. The Carbonatites of the Central Tuva: their geological structure, mineral and chemical composition. Geologiya Rudnykh Mestorozhdenii 47 (4), 360–382.

Platov, V.S., Tereshenkov, V.G., Savchenko, A.A., Busuyek, S.M., Anosov, G.B., Polyansky, S.A., 2000. Explanatory Note to the State Geological Map of the Russian Federation with Scale 1:200,000 to the Sheet M-48-VI of the Selenga Series [in Russian]. Moscow–Saint Petersburg.

Prokopyev, I.R., Borisenko, A.S., Borovikov, A.A., Pavlova, G.G., 2016. Origin of REE-rich ferrocarbonatites in southern Siberia (Russia): implications based on melt and fluid inclusions. Mineral. Petrol. 110 (6), 845–859.

Prokopyev, I.R., Doroshkevich, A.G., Ponomarchuk, A.V., Sergeev, S.A., 2017. Mineralogy, age and genesis of apatite-dolomite ores at the Seligdar apatite deposit (Central Aldan, Russia). Ore Geol. Rev. 81 (1), 296–308.

Prokopyev, I.R., Doroshkevich, A.G., Redina, A.A., Obukhov, A.V., 2018. Magnetite-apatite-dolomitic rocks of Ust-Chulman (Aldan shield, Russia): Seligdar-type carbonatites? Mineral. Petrol. 112 (2), 257–266.

Ripp, G.S., Kobylkina, O.V., Doroshkevich, A.G., Sharakshinov, A.O., 2000. The Late Mesozoic Carbonatites of the Western Transbaikalia [in Russian]. BNTc SO RAN, Ulan-Ude.

Ripp, G.S., Izborodin, I.A., Doroshkevich, A.G., Lastochkin, Ye.I., Rampilov, M.O., Sergeyev, S.A., Travin, A.V., Posokhov, V.F., 2013. Chronology of the formation of the gabbro-syenite-granite series of the Oshurkovo pluton, western Transbaikalia. Petrology 21 (4), 375–392.

Ripp, G.S., Doroshkevich, A.G., Lastochkin, Ye.I., Izborodin, I.A., 2014. Isotope and geochemical characteristics of rocks from the Os-

hurkovo apatite-bearing massif, Western Transbaikalia. Geochem. Int. 52 (4), 271–286.

Ripp, G.S., Izborodin, I.A., Rampilov, M.O., Lastochkin, E.I., Doroshkevich A.G., Khromova, E.A., 2018. A new type of rare-earth mineralization in the Western Transbaikalia. Otechestvennaya Geologiya, No. 3, 9–21.

Ruberti, E., Enrich, G.E., Gomes, C.B., Comin-Chiaramonti, P., 2008. Hydrothermal REE fluorocarbonate mineralization at Barra do Itapirapua, a multiple stockwork carbonatite, Southern Brazil. Can. Min. 46 (4), 901–914.

Samson, I.M., Liu, W.N., Williams-Jones, A.E., 1995. The nature of orthomagmatic hydrothermal fluids in the Oka carbonatite, Quebec, Canada: Evidence from fluid inclusions. Geochim. Cosmochim. Acta 59 (10), 1963–1977.

Sharp, Z.D., 1990. A laser-based microanalytical method for the in situ determination of oxygen isotope ratios of silicates and oxides. Geochim. Cosmochim. Acta 54 (5), 1353–1357.

Shironosova, G.P., Prokopyev, I.R., 2017. Behavior of REE+Y in the fluoride-chloride-sulfate-carbonate media at hydrothermal stages of alkaline magmatic complexes according to the thermodynamic modeling. Izvestiya Tomsk. Politechn. Univ. Inzhiniring Georesursov 328 (12), 75–83.

Shironosova, G.P., Prokopyev, I.R., 2018. The coefficients distribution of REE-Y among minerals and the cooled fluid abundant with the sulphate sulfur (thermodynamic modelling). Izvestiya Tomsk. Politechn. Univ. Inzhiniring Georesursov 329 (10), 6–18.

Smith, M.P., Henderson, P., Campbell, L.S., 2000. Fractionaton of the REE during hydrothermal processes: constraints from the Bayan Obo Fe–REE–Nb deposit, Inner Mongolia, China. Geochim. Cosmochim. Acta 64 (18), 3141–3160.

Smith, M., Kynicky, J., Xu, C., Song, W., Spratt, J., Jeffries, T., Brtnicky, M., Kopriva, A., Cangelosi, D., 2018. The origin of secondary heavy rare earth element enrichment in carbonatites: Constraints from the evolution of the Huanglongpu district, China. Lithos 308–309, 65–82.

Sun, S.-s., McDonough, W.F., 1989. Chemical and isotopic systematics of oceanic basalts: implications for mantle composition and processes, in: Saunders, A.D., Norry, M.J. (Eds.), Magmatism in the Ocean Basins. Geol. Soc. London. Spec. Publ. 42, 313–345.

Tao, F., Yuzhuo, Q., Xiuhua, Q., 1996. Carbon and oxygen isotopic characteristics of REE-fluorocarbonate minerals and their genetic implications, Bayan Obo deposit, Inner Mongolia, China. Chin. J. Geochem. 15 (1), 82–86.

Travin, A.V., Yudin, D.S., Vladimirov, A.G., Khromykh, S.V., Volkova, N.I., Mekhonoshin, A.S., Kolotilina, T.B., 2009. Thermochronology of the Chernorud granulite zone, Ol'khon Region, Western Baikal area. Geochem. Int. 47 (11), 1107–1124.

Tropper, P., Manning, C.E., Harlov, D.E., 2011. Solubility of $CePO_4$ monazite and YPO_4 xenotime in H_2O and H_2O–NaCl at 800 °C and 1 GPa: Implications for REE and Y transport during high-grade metamorphism. Chem. Geol. 282 (1–2), 58–66.

Tropper, P., Manning, C.E., Harlov D.E., 2013. Experimental determination of $CePO_4$ and YPO_4 solubilities in H_2O–NaF at 800 °C and 1 GPa: implications for rare earth element transport in high-grade metamorphic fluids. Geofluids 13 (3), 372–380.

Wall, F., Barreiro, B.A., Spiro, B., 1994. Isotopic evidence for late-stage processes in carbonatites: rare earth mineralization in carbonatites and quartz rocks at Kangankunde, Malawi. Mineral. Mag. 58A, 951–952.

Williams-Jones, A.E., Samson, I.M., Olivo, G., 2000. The genesis of hydrothermal fluorite-REE deposits in the Gallinas Mountains, New Mexico. Econ. Geol. 95 (2), 327–341.

Williams-Jones, A.E., Migdisov, A.A., Samson, I.M., 2012. Hydrothermal mobilisation of the rare earth elements—a tale of "Ceria" and "Yttria". Elements 8 (5), 355–360.

Xie, Y., Hou, Z., Yin, S, Dominy, S., Xu, J., Tian, S., Xu, W., 2009. Continuous carbonatitic melt–fluid evolution of a REE mineralization system: Evidence from inclusions in the Maoniuping REE Deposit, Western Sichuan, China. Ore Geol. Rev. 36 (1–3), 90–105.

Editorial responsibility: E.V. Sklyarov